Bacteriophage M13 Aggregation on a Microhole Poly(ethylene-terephthalate) Substrate Produces an Anionic Current Rectifier: Sensitivity Towards Anionic *versus* Cationic Guests

Budi Riza Putra [1,2], Katarzyna Szot-Karpińska [3], Patryk Kudła [3], Han Yin [1], Jacob A. Boswell [1], Adam M. Squires [1], Marcelo A. Da Silva [1], Karen J. Edler [1], Philip J. Fletcher [4], Stephen C. Parker [1], and Frank Marken*[1]

[1] *Department of Chemistry, University of Bath, Claverton Down, BA2 7AY, UK*
[2] *Department of Chemistry, Faculty of Mathematics and Natural Sciences, Bogor Agricultural University, Bogor, West Java, Indonesia*
[3] *Institute of Physical Chemistry, Polish Academy of Sciences, Kasprzaka 44/52, 01-224 Warsaw, Poland*
[4] *Material & Chemical Characterisation Facility MC[2], University of Bath, Bath BA2 7AY, UK*

Proof to F. Marken (f.marken@bath.ac.uk)

Abstract

Bacteriophage material (M13, wild-type) deposited as a film onto a poly-ethylene-terephthalate (PET) substrate (6 μm thick with a 20 μm diameter laser-drilled microhole) has been investigated for ion conductivity and ionic current rectification effects for potential applications in membranes. The M13 aggregate membrane forms under acidic conditions (in aqueous 10 mM acids) and behaves like a microporous anion conductor with micropores defined by the packing of cylindrical virus particles. Asymmetric deposition on the PET film substrate in conjunction with semi-permeability leads to anionic diode behaviour. Typical rectification ratio values are around 10 (determined at +/-1V) in aqueous 10 mM acids. Cationic guest species (aqueous Cu^{2+}, Co^{2+}, Ag^{+}) consistently lead to a rectification minimum at 0.5 mM guest concentration. In contrast, anionic guest species (indigo carmine) lead to a similar rectification minimum already at 5 μM concentration. The behaviour is proposed to be associated with cation exclusion effects on transport.

Keywords: bacteriophage; electrostatic interactions; double layer; nanofluidics; nanopore; ion transfer; sensor

1. Introduction

Phage materials provide extraordinarily robust nanostructures when exposed to heat or to chemical changes (organic solvents, alkali, acids, etc.) or when applied as templates[1] or as natural scaffolds.[2] Due to their ability to exactly replicate, they can produce structurally well-defined nanomaterials at the molecular limit. Many applications of phage materials are based on the end/surface groups being covered with proteins with encoded selectivity (phage display[3,4] or sensor development[5]), but many other aspects of the atomic level design of phage materials are also appealing for applications. Phage materials have been employed in electrochemical processes.[6,7,8,9] For bacteriophage M13, the uniform surface chemistry based on capsid protein pVIII (see Figure 1) could offer a well-defined surface charge for future membrane applications, if the virus particles can be aggregated into dense microporous films. Applications could be, for example, in membrane separation, in ionic nanofluidic devices,[10] or in desalination and water purification.[11] A first necessary step in the formation of M13 phage membranes is aggregation.

Chemical modification of M13 phage material[12] as well as encapsulation[13] have been reported. Genetic modification offers a generic tool to modify the structure, morphology, and surface functionalisation.[14] The geometry of the M13 virus particles is linked mainly to the protein shell, which packs densely to give a tubular morphology with 6.6 nm diameter and with typically 880 nm length (see Figure 1). A lot is known about the molecular structure of bacteriophage M13.[15] The phages are filamentous in appearance and the surface coating is dominated by a single protein, pVIII.[16] Structurally, the repeat length along the cylindrical object is 2.7 nm with 10 pVIII proteins contributing the one repeat length (see Figure 1C). Given the radial diameter 6.6 nm and assuming cylindrical geometry, the exposed surface area per pVIII protein is readily estimated as 5.6 nm^2. The pVIII protein has a positive region (inwardly directed to interact with embedded DNA) and at the opposite end a negative region (outward directed) to define the surface.[17] The pVIII protein represents 98% of the virus mass and can be written as a sequence of 50 amino acids, some of which are responsible for the surface charges.[18,19]

The iso-electric point of M13 phage is at approximately 4.2.[20] The isoelectric point is linked to the pK_A of bacteriophage M13 particles, which is dependent on the outside protonation of the protein shell. The main protein shell in the cylindrical section of the phage, pVIII, shows a slight excess positive charge internally with some more negatively charged functional groups exposed to the outside of the virus. Exposed charged groups on the outside surface are the NH_2 terminus, Glu2, Asp4, Asp5, Lys8, Asp12, and Glu20.[16] At a pH of 7, Lys would be positive and both Asp and Glu are negative (net -3 charge). However, at a pH of 2 (in the presence of 10 mM aqueous acid), only the +2 surface charge should remain. This excess positive charge defines a microchannel (see the small circle in Figure 1C) that is formed when packing the cylindrical virus particles.

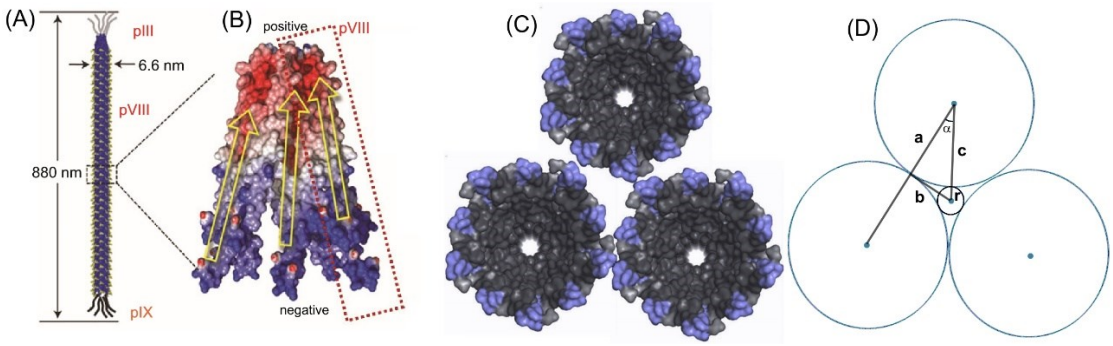

Figure 1. (A-C) Drawing of the M13 bacteriophage (Reproduced with permission from reference [18]. Copyright 2012 Springer-Verlag). (B) Packing of the pVIII protein with positive excess charge internally (interacting with DNA) and negative excess charge externally (interacting with electrolyte). (C) Schematic drawing of three virus particles (in cross section) packing to give a central microchannel. (D) Calculation of the microchannel diameter.

Figure 1D describes the geometry assumed for the densest packing of the filamentous virus particles. The diameter of the microchannel (2r) for ion transport can be related to the diameter of the virus particles (2a = 6.6 nm) and the angle $\alpha = 30^o$. The radius is given by r = c-a, which can be rewritten as $r = a/\cos\alpha - a = a(1/\cos\alpha - 1)$. This suggests that r is 15.5% of c, and therefore the diameter for the ion conducting channel is approximately 2r = 1 nm. This type of channel is narrow, but sufficient for ion transport. With a typical Debye layer estimate of $\kappa^{-1} = 0.3/I^{0.5} = 3$ nm (here I is the ionic strength[21])

in a 10 mM aqueous solution, strong cation exclusion can be expected (at pH 2). The virus aggregation should result in a semi-permeable anion conductor characteristics.

In this report, aggregation of M13 wild-type phage is demonstrated to give membrane-forming aggregates in aqueous 10 mM acids. The intrinsic micro-channel system formed between cylindrical phage material offers ion transport pathways. The asymmetric deposit of the phage material on a microhole in a PET film substrate results in ionic rectifier behaviour. Due to the competing potential-driven flow of anions and cations in these microchannels, distinct effects for cationic and anionic guest species (rectification minima) are observed. It is suggested that in the future, phage materials (in particular phage with further surface modification) could be employed in ionically switched sensors or in novel biological materials for separation and membrane technologies.

2. Experimental

2.1. Chemical Reagents. A wild bacteriophage M13 KE lysate was supplied from New England Biolabs, NEB. For the experiments the M13 phage were multiplied on *Escherichia coli* ER2738 (NEB) according to the NEB protocol.[3] The concentration of the multiplied M13 phage was 1.04×10^{14} plaque-forming units per mL (PFU/mL). Hydrochloric acid, nitric acid, sulphuric acid, perchloric acid, phosphoric acid, agarose, copper (II) perchlorate, cobalt (II) perchlorate, silver nitrate, and indigo carmine were obtained from Sigma-Aldrich Ltd. and used without further purification. Solutions were prepared under ambient conditions in volumetric flasks with ultrapure water resistivity of 18.2 MΩ cm (T = 20 +/- 2 ºC) from an ELGA Purelab Classic System for water filtration.

2.2. Instrumentation. Transmission electron microscopy (TEM) was performed with a JEOL JEM-2100 Plus instrument with 200 kV maximum operating voltage. Scanning electron microscopy (SEM) was performed with a JEOL JSM-6480LV SEM. The zeta-potential for the bacteriophage M13 solution was measured on a Zetasizer Nano ZS (Malvern Instruments Ltd, Malvern, UK). Scattering analysis for the bacteriophage M13 and HCl-treated phage M13 solution was perfomed using small angle X-ray scattering (SAXS) system from Anton Paar. The scattering vector (Q) was calculated

using $Q = 4\pi \sin\theta/\lambda$, where θ is half of the scattering angle, λ is the x-ray wavelength (1.54 Å). 1D scattering patterns of intensity *vs*. *Q* were fitted to a cylinder fit with SASView 4.2.2.

Electrochemical data (for both voltammetry and chronoamperometry) were recorded at T = 20 ± 2 ºC on a potentiostat system (Ivium Compactstat, Netherland). A classic 4-electrode electrochemical cell configuration was employed.[22] The membrane separates two tubular half-cells (15 mm diameter), one with Pt wire working and KCl-saturated calomel (SCE) sense electrode, and the other one with SCE electrode and Pt wire counter electrode. In electrochemical measurements the working electrode was always located on the side of the bacteriophage M13 film deposit.

2.3. Procedures. The polyethylene-terephthalate (PET) films of 6 μm thickness with laser-drilled 20 μm diameter microhole were obtained from Laser-Micro-Machining Ltd., Birmingham, UK. A microscopy glass slide was pre-coated with a thin layer of 1% agarose gel. The PET film was placed onto the gel to stop liquid entering and running through the microhole (and to define the interface within the microhole). A 10 μL volume of bacteriophage M13 solution (1.04×10^{14} PFU/mL) was applied to the surface and with a glass rod the bacteriophage M13 solution was spread evenly over ca. 1 cm^2 of the PET surface. After drying of the bacteriophage M13 deposit, 10 μL volume of bacteriophage M13 was applied once again to the PET film. Finally, the PET film was removed from the agarose gel and stored under dry conditions. For electrochemical measurements the film was mounted in a U-cell between the two glass flanges with the help of some Dow-Corning vacuum grease as sealant. Reproducibility of currents for multiple devices is generally good (typically ±10 %, with variations probably mainly due to slight variations in the film thickness). New films were employed for each set of experiments. Before use, every new film was tested in aqueous 10 mM HCl to ensure reproducibility in both current and rectification.

Data from light scattering experiments (Malvern Zetasizer Nano ZS) are shown in Table 1. Bacteriophage M13 exhibits a negative zeta potential -18 mV in aqueous 10 mM NaCl. The average size of 168 nm from DLS measurements assumes spherical particles, so is approximately consistent with dissolved cylindrical material where

diameter and length are very different (*vide infra* [16]). In addition the DLS measurement records the hydrodynamic diameter, including the shell of ions and water around the particles, rather than the bare particle size. In contrast, in aqueous 10 mM HCl aggregation occurs, the Z-average diameter appears increased (consistent with aggregation), and the zeta potential changes to +20.6 mV indicative of surface protonation and negative counter anions weakly associated to the surface.

Table 1. Zeta potential measurements and diameter measured using dynamic light scattering in 10 mM NaCl and in 10 mM HCl (errors expressed as standard deviation for triplicate measurements).

Sample		Z-average diameter / nm	Zeta-potential / mV
M13 bacteriophages	in NaCl 10 mM	168 ± 20	-18.0 ± 2.4
	in HCl 10 mM	1145 ± 152	+20.6 ± 3.7

Electron optical measurements (TEM, see Figure 2) employed uranyl stained M13 phages and suggest a highly filamentous structure. Material deposited from distilled water appears open and distributed (Figure 2A), but after deposition from aqueous HCl (Figure 2B,C) aggregation can be seen and the formation of bundles of filamentous material.

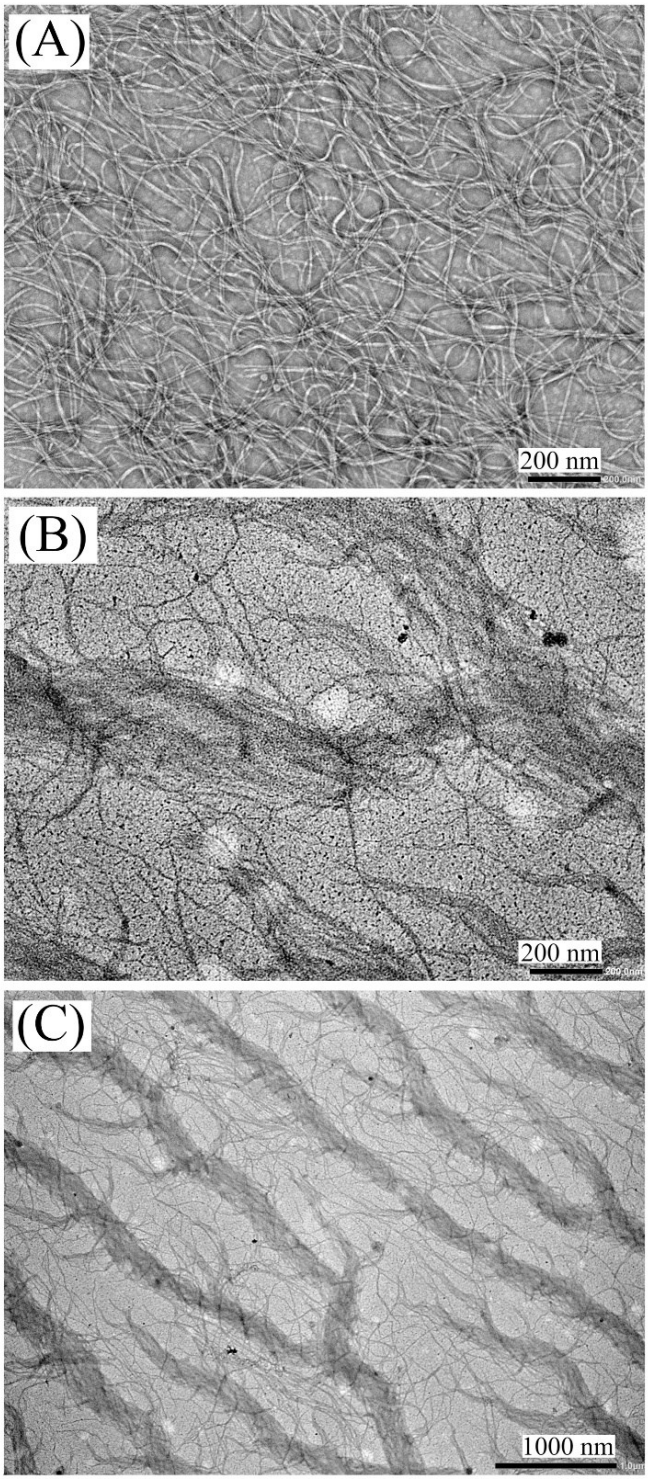

Figure 2. (A) TEM image for M13 phage deposited from aqueous dispersion. (B,C) TEM images for M13 phage deposited and aggregated when exposed to aqueous 10 mM HCl.

From SAXS data M13 phage geometric properties can be obtained in the absence and in the presence of HCl. Figure 3 shows data sets obtained in water (blue data) and with addition of HCl (green data). Also shown are cylinder model fits (using the modelling

software SASView[23]) for these two data sets. As expected, the data sets closely agree. For the water sample the diameter is 7.2 +/- 0.8 nm with a typical length of 24 +/- 6 nm. In the presence of HCl data fitting suggests a diameter of 7.1 +/- 1.1 nm and a length of 19 +/- 5 nm. The observed diameter is in good agreement of the literature value of 6.6 nm (31.5 nm was observed for the apparent length).[24]

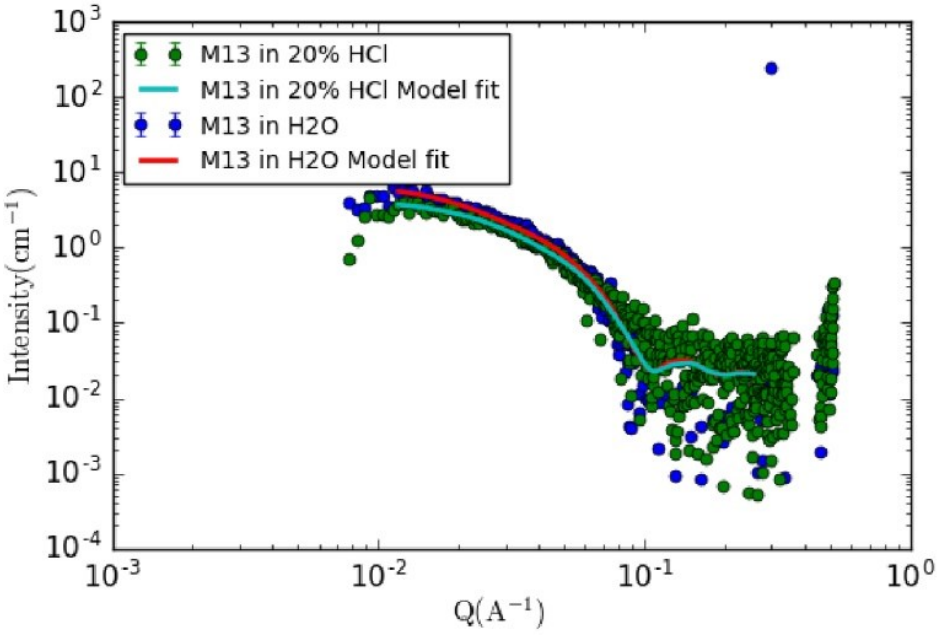

Figure 3. SAXS data for M13 phage in water (blue points) and in aqueous HCl (green points). Cylinder model fits are shown to closely agree for the two data sets. Limit Q plotting range to the fitting range (~0.08 – 0.5).

When imaging the M13 phage deposit with scanning electron microscopy (SEM, see Figure 4), the asymmerty between the bottom or the PET film (Figure 4A) and the top of the PET film (Figure 4B) is observed. Here, the M13 phage deposits were exposed to 10 mM HCl prior to imaging in order to demonstrate the aggregation to give a dense asymmetric deposit. The cross-sectional image in Figure 4C suggests uneven films of about 10 μm thickness.

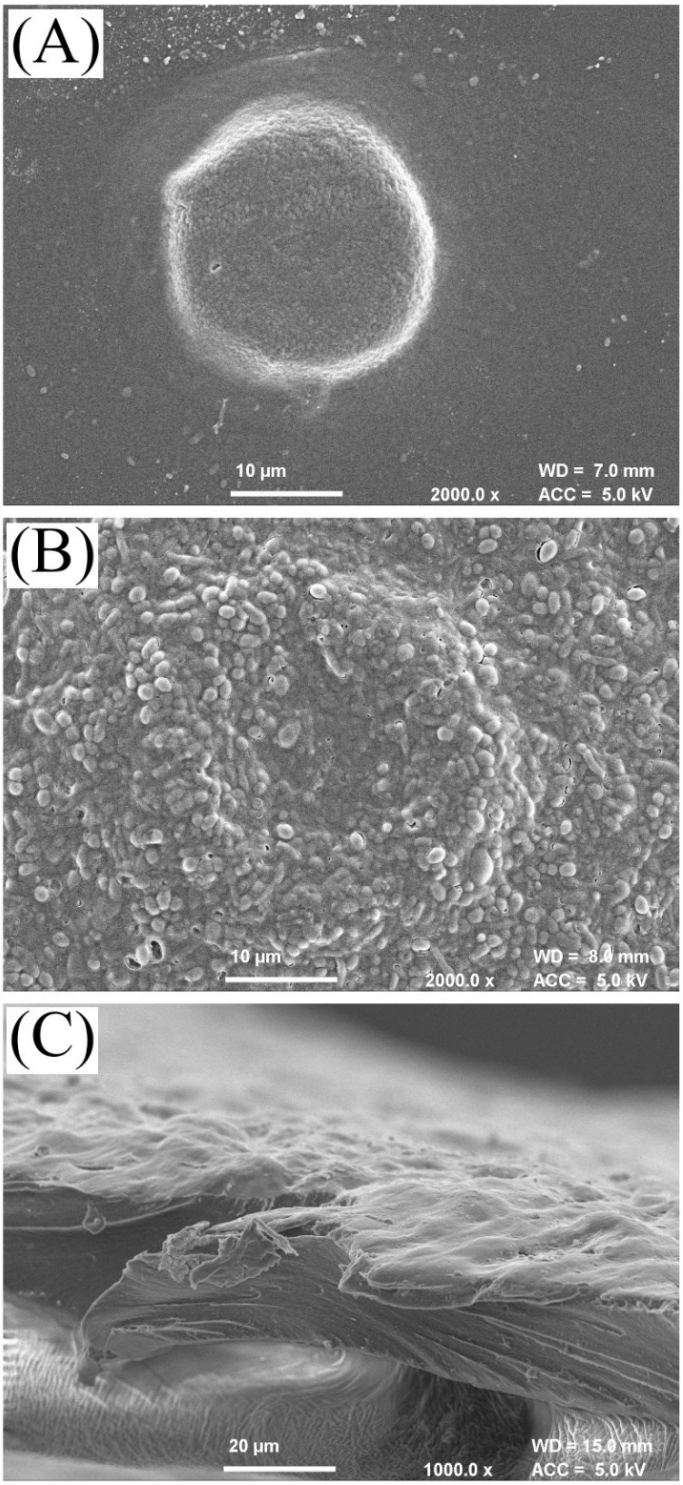

Figure 4. (A) SEM image for M13 phage deposited from aqueous dispersion onto a PET microhole substrate (and aggregated by exposure to 10 mM HCl). Bottom view showing the PET recess (20 µm diameter) with M13 phage deposit below. (B) SEM image as before, but top view of M13 phage deposit (aggregated by exposure to aqueous 10 mM HCl). (C) Freeze-fracture cross-sectional image of the approximately 10 µm thick phage deposit on PET.

3. Results and Discussion

3.1. Phage Deposits Lead to Ionic Rectifier Behaviour: Aqueous Acids

When exposed to neutral or alkaline aqueous electrolyte, M13 phage material does not form mechanically stable assemblies. Deposits simply dissolve. However, in acidic solution environments, a permanent membrane-like material is produced, which behaves like an anion conductor. Figure 5A shows the measurement cell with M13 phage deposited asymmetrically (see experimental) onto a poly-ethylene-terephthalate (PET) film with a 20 μm diameter microhole. The thickness of the phage deposit is not well-controlled and estimated here to be approximately 10 μm. Experiments with additional phage material (*i.e.* a thicker film) did not significantly change the behaviour, although thinner films are mechanically more fragile. The M13 film is placed between two electrolyte reservoirs with the working and sense electrode on the right (facing the M13 deposit, see Figure 5A) and the reference and counter electrode on the opposite side. In this configuration, the potential is applied between reference and sense electrodes (both SCE) and the associated current flows between working and counter electrode.

Voltammetric data in Figure 5B show the effect of the M13 deposit on ion flux. The empty microhole produces an Ohmic response (R = 118 kΩ) indicative of the specific resistivity of the aqueous HCl electrolyte with contributions from the cylindrical region and from access diffusion-migration.[25] With the M13 phage deposit present, two distinct potential domains are observed. In the positive potential range, the ion flux is much diminished consistent with a "closed" diode state. In the negative potential range, the current is similar to that observed for the empty microhole consistent with an "open" diodes state. This type of behaviour is observed usually for ion-conducting materials with anion semi-permeable characteristics[26] and consistent with the protonated M13 phage material allowing only mobile anions to flow in microchannels in between the virus particles. Protonation of the phage surface results in mobile anion counter charges in a Debye layer that is present within channels between cylindrical strands of the phage material (see Figure 6). Cation transport is inhibited due to cation exclusion.

The asymmetric deposition of the phage deposit in this case is important to induce the desired rectification effects. Experiments with symmetric ionomer deposits only result in Ohmic behaviour.[27] Also, the effect of an imbalance in ionic strength on the two sides of the electrochemical cell has been reported to affect the rectification effect.[28]

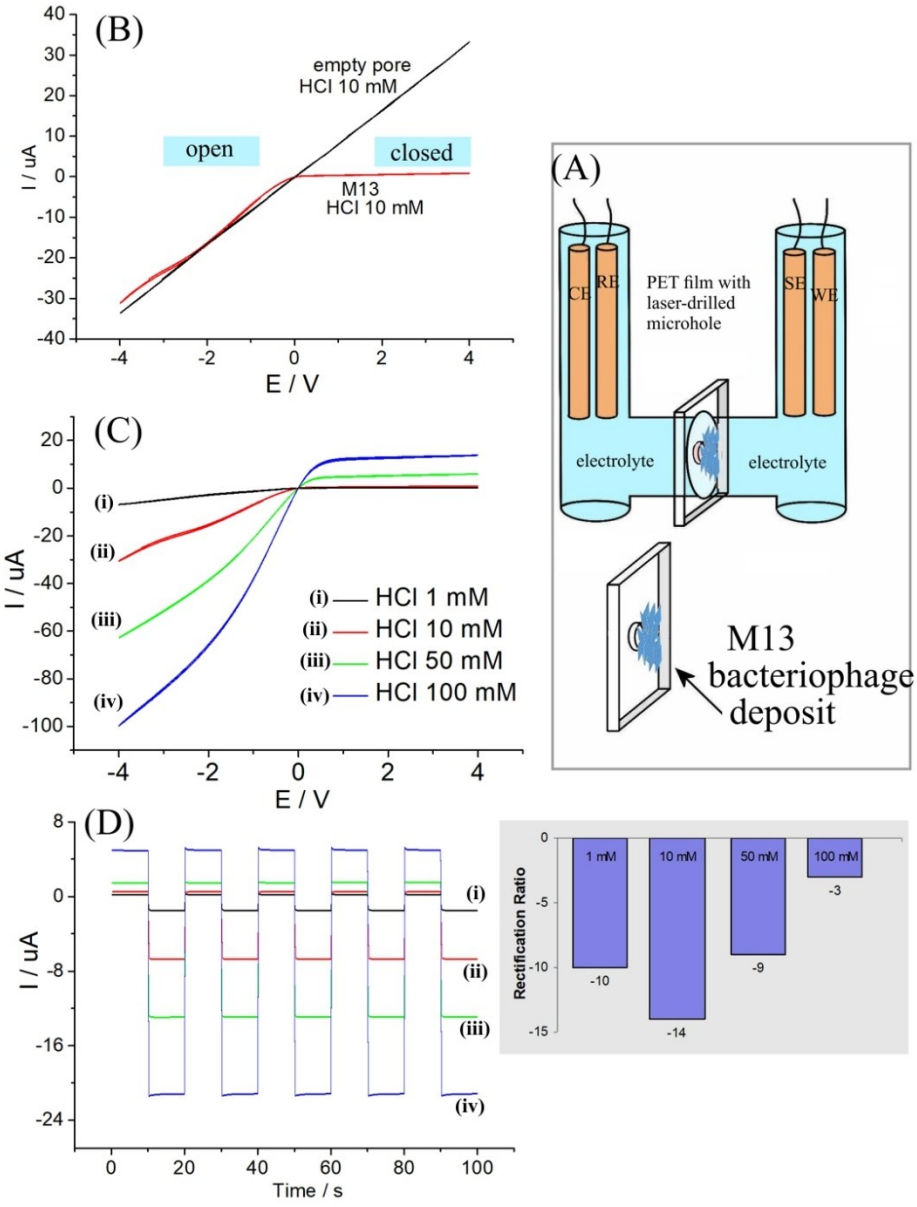

Figure 5. (A) Schematic drawing of the 4-electrode measurement cell with an M13 phage deposit asymmetrically on a 6 µm thick PET film with 20 µm diameter microhole. (B) Voltammetric signal in 10 mM HCl (scan rate 50 mVs^{-1}) comparing the empty microhole (behaving like a resistor) and the microhole with M13 phage deposit (behaving like an anionic diode). (C) Voltammetry data (scan rate 50 mVs^{-1}, M13 phage deposit) obtained in (i) 1 mM, (ii) 10 mM, (iii) 50 mM, and (iv) 100 mM HCl. (D) Chronoamperometry data (switching between -1V and +1V) for (i) 1 mM, (ii) 10 mM, (iii) 50 mM, and (iv) 100 mM HCl.

In order to better explain the observed diode effect, it is necessary to consider anion transport and the electrolyte concentration within the microhole region in the PET film.[29] For an anion conductor and with positive potential applied to the working electrode, anions diffuse from bulk solution to the PET microhole. Within the microhole this results in electrolyte depletion and a high resistance (see Figure 6, "closed" state). Here, depletion causes removal of HCl from the microhole region and this is linked to loss of some surface protonation also within the phage film. The adjacent phage material is affected (see Figure 6) with deprotonation locally further increasing the resistance and severely limiting the flow of current. When applying a negative potential to the working electrode, anions are driven through the phage material in opposite direction to result in an increase in electrolyte concentration within the microhole region and therefore lower resistance (see Figure 6, "open" state). Protons also re-enter the previously depleted region in the phage material to provide a more positive surface charge and improved anion conductivity.

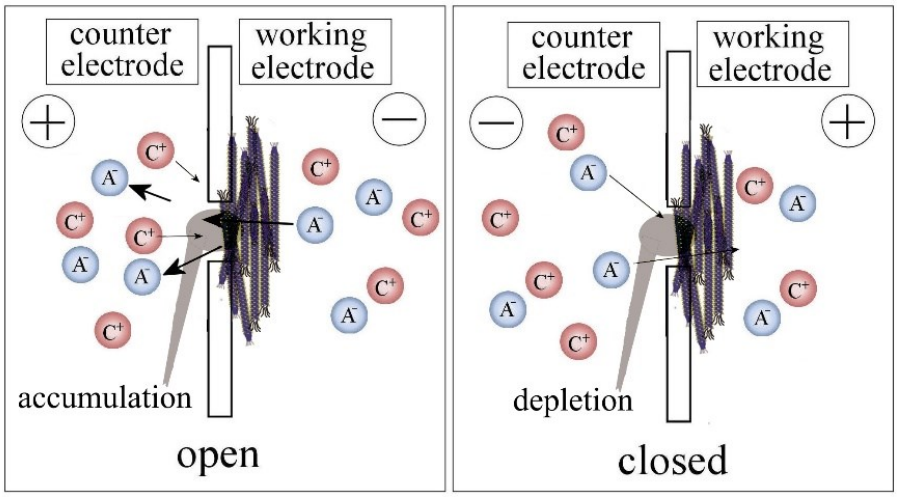

Figure 6. Schematic drawing of the ion movement and accumulation/depletion effects induced in the M13 phage diode by externally applied potentials.

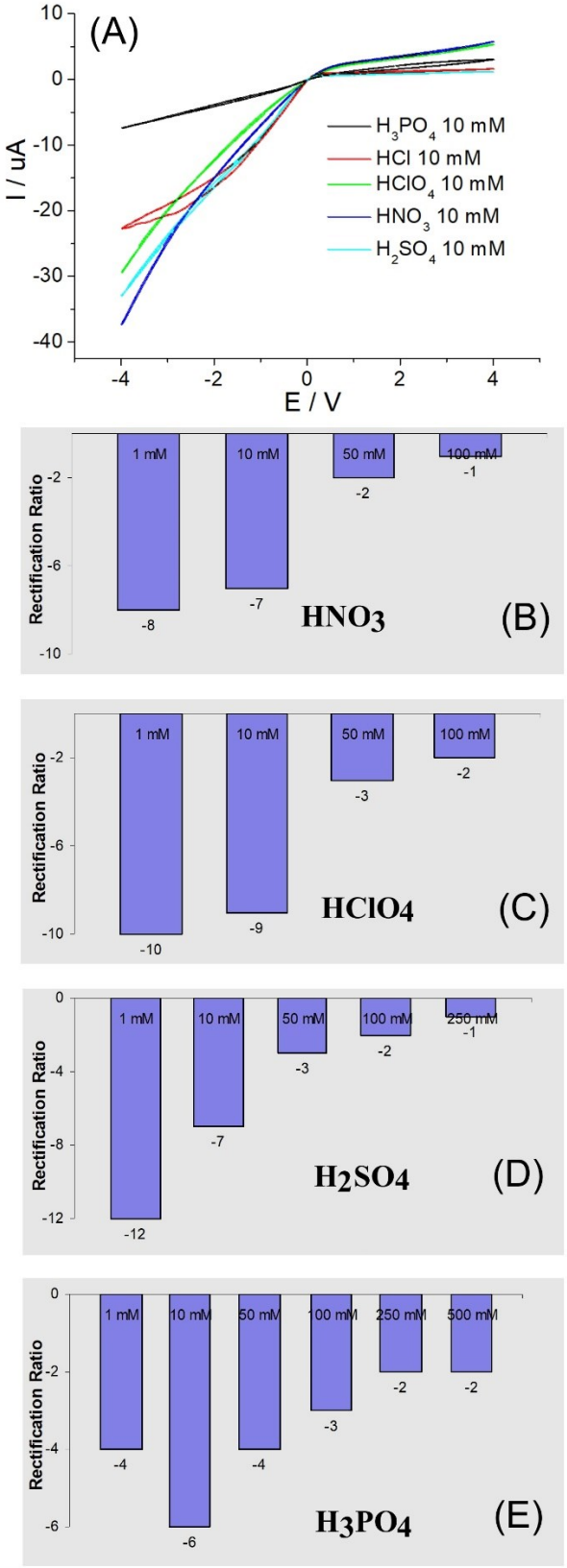

Figure 7. (A) Voltammograms (scan rate 100 mVs^{-1}) in 10 mM mineral acids (H_3PO_4, $HClO_4$, H_2SO_4, HNO_3). Also shown are bar plots of rectification ratio data (obtained by chronoamperometry at +1V and -1V) for (B) HNO_3, (C) $HClO_4$, (D) H_2SO_4, and (E) H_3PO_4.

The resulting current rectification effects can be summarised in the rectification ratio (here determined at +/-1 V). Figure 5D shows transient (chronoamperometry) data for different HCl concentrations. Note that the time for on/off switching is relatively short, approximately 1 s, consistent with fast-moving protons. With an increase in concentration of aqueous HCl, a net decrease in rectification ratio is observed (although generally the ion flux is increased, see Figure 5C). It seems likely that loss of semi-permeability within the phage material at higher ionic strength is the reason for this decrease in rectification effect. At an ionic strength of $I = 0.1$ M the approximate Debye length is reduced to $\kappa^{-1} = 0.3/I^{0.5} = 0.95$ nm and more cations can enter the microchannels.

When repeating voltammetry and chronoamperometry experiments with M13 phage deposits in the presence of different types of inorganic acids (with concentrations ranging from 1 mM to 100 mM or higher), a very similar picture emerges in all cases. A summary of voltammetry and rectification ratio data (Figure 7) shows that maximum rectification occurs at 1 mM or 10 mM electrolyte concentration with a rectification ratio of typically 10 (for +1V/-1V chronoamperometry). An increase in ionic strength generally causes a loss in rectification effect. It is of interest to explore the additional effects of other ionic solution species on the rectification effect. In the next section the focus is on the effect of additional cationic species on the rectification effect.

3.2. Phage Ionic Rectifier Behaviour: Cationic Guests

Initial exploratory experiments conducted with Fe(III) or Cu(II) cations in aqueous 10 mM hydrochloric acid suggested a negligible effect of these species on ion transport within the phage material, probably due to the formation of anionic complexes such as $FeCl_4^-$ or $CuCl_4^{2-}$. The appearance of voltammetric data and the rectification effect were essentially unaffected. However, in the absence of chloride (here in aqueous 10 mM $HClO_4$), additional cationic species can result in a characteristic change in ionic rectifier behaviour.

In a non-coordinating environment, here 10 mM $HClO_4$, Cu^{2+} cations do change the voltammetric behaviour of the M13 phage diodes. Figure 8 shows a summary of data for a concentration range from 62 μM to 5 mM $Cu(ClO_4)_2$ added on the working

electrode side (that is, the side with the phage material deposit). Initially, the current in the open state of the diode decreases with Cu^{2+} addition. Upon increasing the concentration, a minimum in current response is reached with 0.5 mM $Cu(ClO_4)_2$ added. The minimum in open state current coincides with a minimum in rectification ratio. A plot is shown for the rectification ratio at +/-1 V and for +/-4 V applied potential. The higher voltage results in a more clear representation of the diode character. It can be assumed that the uptake of Cu^{2+} into the micropore channels created by the M13 phage material is responsible for a change in semi-permeability. With 0.5 mM $Cu(ClO_4)_2$ concentration, the diode effect is almost lost, possibly due to Cu^{2+} binding to amine and/or carboxylate sites at the virus surface and thereby lowering the surface charge and anion conductivity. Perhaps surprisingly, the diode effect recovers when further increasing the Cu^{2+} concentration. A characteristic minimum in rectification is observed.

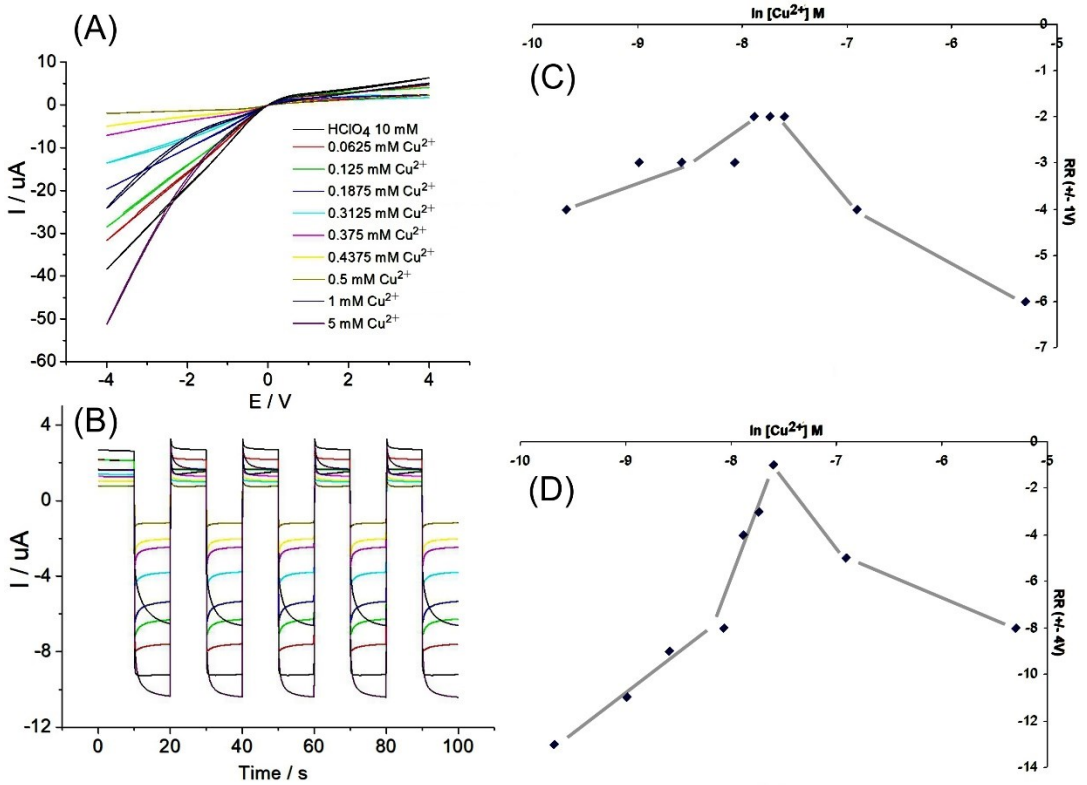

Figure 8. (A) Cyclic voltammograms (scan rate 50 mV s^{-1}) for M13 phage deposit on a 20 μm diameter PET microhole immersed in 10 mM $HClO_4$ with additions of Cu^{2+}. (B) Chronoamperometry data (switching between -1 and +1 V). (C) Plot of rectification ratio (at +/-1 V) versus copper concentration. (D) As before but for +/-4 V chronoamperometry. Lines are shown to guide the eyes.

It is interesting to explore the ion flux as a function of time in chronoamperometry experiments. Figure 8B shows data as a function of added $Cu(ClO_4)_2$. In the absence of Cu^{2+} a fast transient occurs with equilibrium reached almost instantly (proton diffusion is relatively fast and changes in phage protonation are rapidly adjusted after switching the potential). Once small amounts of Cu^{2+} are added the transients (both positive and negative) display falling transient characteristics, which suggests that the current is initially high to then drops down to a dynamic equilibrium value (consistent with a low population of less mobile Cu^{2+} in the phage material competing with the faster protonation process). However, when going beyond the point at 0.5 mM Cu^{2+} the transients show rising characteristics. At this point the Cu^{2+} concentration is sufficiently high to dominate the surface charge and to give a Cu^{2+} based anionic diode system with slower transients.

Figure 9 shows data for Co^{2+} obtained under the same conditions. Perhaps surprisingly, the characteristics are very similar to those for Cu^{2+}. The rectification effect is lost with increasing Co^{2+} concentration and at higher than 0.5 mM Co^{2+} concentration the diode effect is recovered, although with rising transient. It can be concluded that both Cu^{2+} and Co^{2+} cation species have essentially the same effect on the protonated phage surface, probably as weakly interacting guests within the micropore channels of the virus deposit.

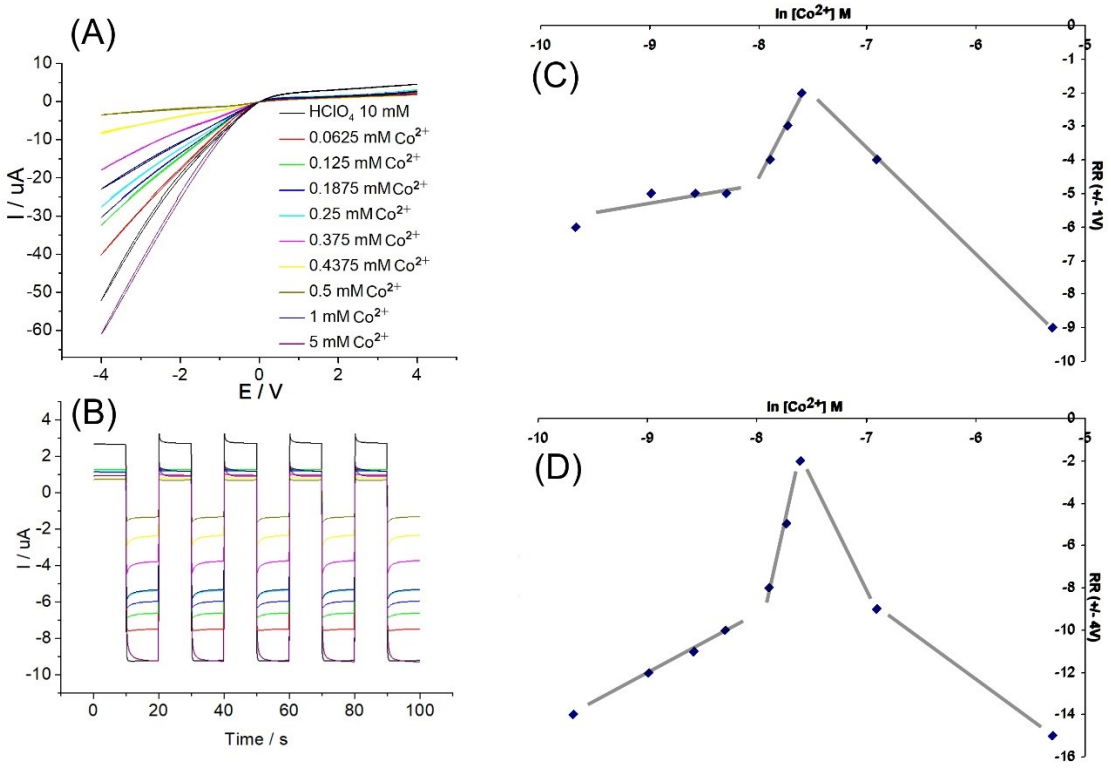

Figure 9. (A) Cyclic voltammograms (scan rate 50 mV s^{-1}) for M13 phage deposit on a 20 μm diameter PET microhole immersed in 10 mM $HClO_4$ with additions of Co^{2+}. (B) Chronoamperometry data (switching between -1 and +1 V). (C) Plot of rectification ratio (at +/-1 V) versus cobalt concentration. (D) As before but for +/-4 V chronoamperometry.

For both, Cu^{2+} and Co^{2+}, it is possible to re-immerse the ionic diode into pure 10 mM $HClO_4$ to recover the original characteristics. That is, the Cu^{2+} or Co^{2+} coordination to the virus surface is probably weak and inconsequential in terms of chemical surface modification of the virus.

When using Ag^+ as cation a more permanent change occurs. Figure 10 summarises the ionic diode characteristics as a function of added Ag^+. Most striking is the similarity in the initial decrease in diode current (and rectification ratio) to a minimum, followed by an increase at approximately 0.5 mM concentration of Ag^+. For Ag^+ the shape of transient responses remains rising even at higher concentrations of Ag^+, but the change in diode behaviour is also permanent with no recovery after going back to aqueous 10 mM $HClO_4$. Both could suggest a more permanent modification of the virus surface and absence of competition with the more mobile protons. It seems likely that Ag^+ can affect surface charge by forming bonds to amine and carboxylate moieties and further

modification by chemical oxidation. Details of virus surface modification by Ag^+ are currently unknown but interaction with silver nanoparticles has been reported.[30] The similarity in the voltammetric behaviour of the diode for Cu^{2+}, Co^{2+}, and Ag^+ suggests closely related mechanisms, probably associated with weak binding of the cation into the double layer of the virus surface. Next, a negatively charged aromatic guest species is shown to lead to substantially different ionic diode characteristics when acting as a guest species in the M13 phage aggregate.

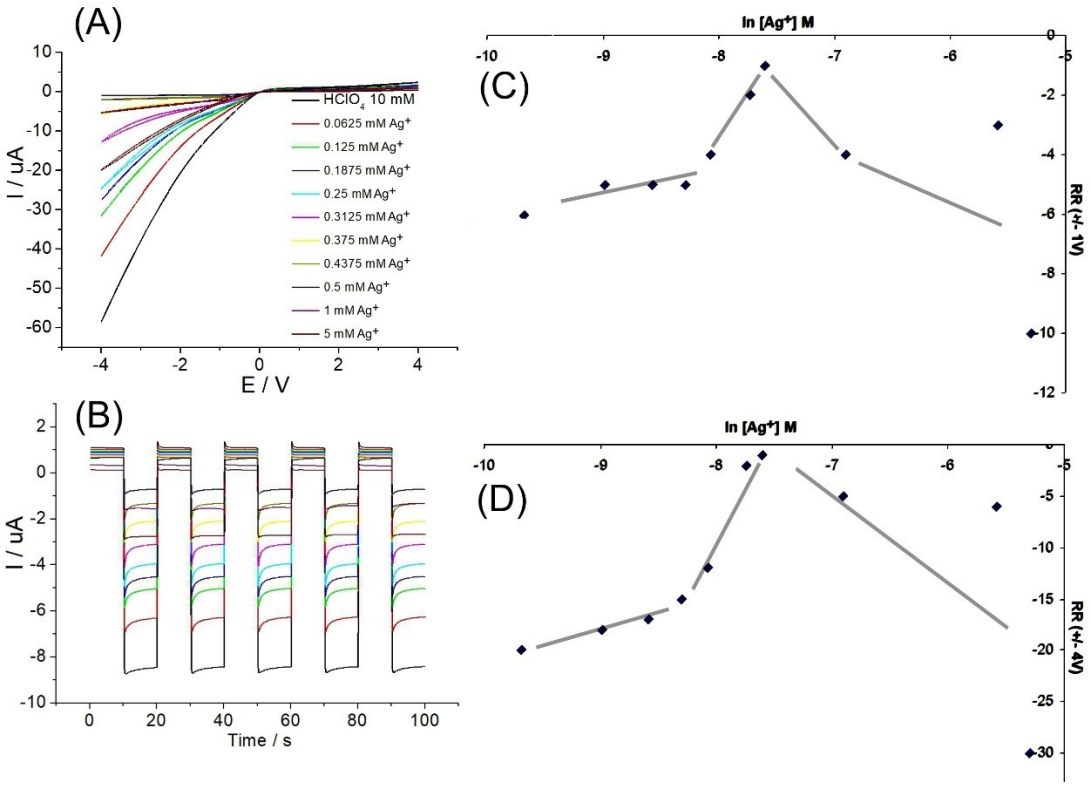

Figure 10. (A) Cyclic voltammograms (scan rate 50 mV s^{-1}) for M13 phage deposit on a 20 μm diameter PET microhole immersed in 10 mM $HClO_4$ with additions of Ag^+. (B) Chronoamperometry data (switching between -1 and +1 V). (C) Plot of rectification ratio (at +/-1 V) versus silver concentration. (D) As before but for +/-4 V chronoamperometry.

3.3. Phage Ionic Rectifier Behaviour: Anionic Guests

Hydrophobic molecules such as indigo carmine (see molecular structure in Figure 11) are likely to bind to the positively charged M13 virus surface and should therefore

strongly affect ion flow and the diode characteristics. This is shown in Figure 11A. The ionic diode behaviour is affected already at concentrations 100 times lower compared to those used for cationic guests (compare Figure 10). When adding indigo carmine, the ionic diode current in the open state lowers to reach a minimum (here at approximately 5 μM indigo carmine) and then recovers when going to higher concentrations. Here, the binding of indigo carmine is likely to directly change the surface charge and to reduce the population of mobile anions (perchlorate) in the microchannel space between virus particles.

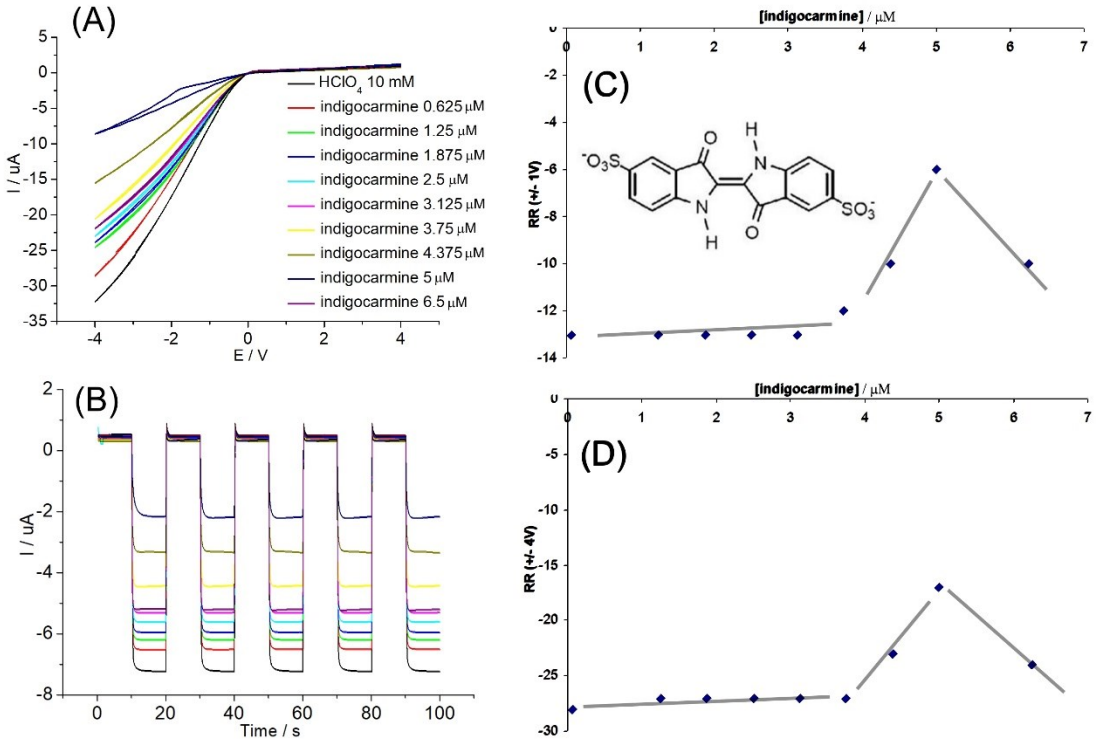

Figure 11. (A) Cyclic voltammograms (scan rate 50 mV s^{-1}) for M13 phage deposit on a 20 μm diameter PET microhole immersed in 10 mM $HClO_4$ with additions of indigo carmine. (B) Chronoamperometry data (switching between -1 and +1 V). (C) Plot of rectification ratio (at +/-1 V) *versus* indigo carmine concentration. (D) As before but for +/-4 V chronoamperometry. Lines are shown to guide the eyes.

Transient data in Figure 11B reveal fast switching between closed and open state consistent with rapid proton exchange in the depletion region of the phage material close to the microhole. The recovery of the anionic diode effect at indigo carmine concentrations higher than 5 μM suggests that indigo carmine remains mobile and can contribute to the rectification effect. In chronoamperometry data Figure 11C), generally

rising transients are observed indicative of absence of competition to the proton uptake/release in the depletion region.

In all cases of guests within the virus deposit the closed diode state appears essentially insensitive, probably due to perchlorate diffusion towards the PET microhole dominating the transport and depletion effect. However, in the open state of the ionic diode the ion transport through the virus deposit is crucial and changes in anion transport are detected as a function of bound guest species.

For the anionic guest, indigo carmine, the low concentration for binding to the virus deposit is consistent with the fact that anion semi-permeability is observed. Guest anions easily enter and bind to the virus surface. This modifies the surface charge leading to loss of diode character. The following increase in diode effect can be explained by considering excess indigo carmine as a mobile species able to permeate through the virus deposit in a way similar to the perchlorate permeation (see Figure 12).

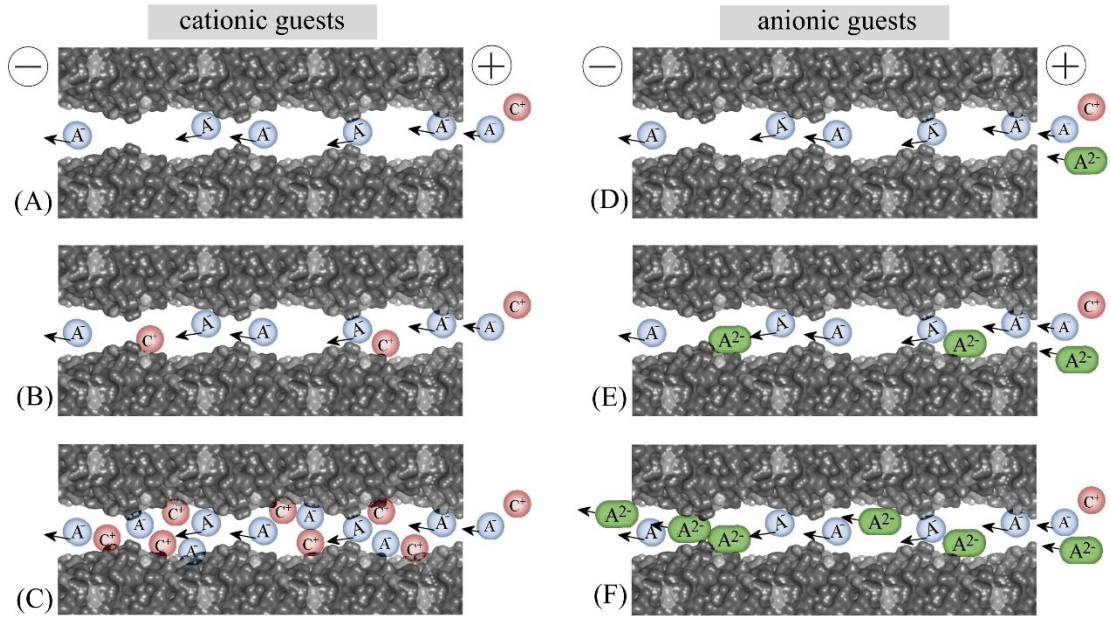

Figure 12. Schematic illustration of (A-C) a cationic guest species entering a microchannel initially with a blocking effect and then at higher concentration with a current enhancing effect. In (D-F) the case of an anionic guest is illustrated with initially a blocking effect followed at higher concentration with a current enhancing effect.

For the cationic guest species initially access to the anion selective virus film is inhibited. At a sufficiently high concentration (here 0.5 mM), the guest cations can enter and interact with the virus material. This threshold is insensitive to the chemical nature of the cations. Once bound to the virus cations can initially lower the rate of transport, but then the diode effect recovers due to dominating anion transport with excess cation binding. The effect of the guest species remains insignificant when the guest species is added into the counter electrode side of the electrochemical cell. Therefore, the interaction of guest with virus appears to require effective exposure of the virus film to the guest solution.

There are many remaining questions about the specificity of binding events to the virus surface, the binding to a wider range of guest species, and the potential of the M13 phage deposits to function as a diode sensor with specific binding ability. More work will be needed to better and more quantitatively understand processes at the virus surface, as a function of double layer conditions, and based on the effects of modifying the virus surface on ionic diode characteristics.

4. Conclusions and Outlook

It has been shown that M13 phage material can aggregate in 10 mM acid and at a pH acidic of the isoelectric point. The resulting phage material forms micropores with cationic surface charges for anion conduction. Semi-permeability (and cation exclusion) is weakened when the concentration of electrolyte is increased.

The observation of semi-permeability resulted in anionic diode behaviour for asymmetrically deposited M13 phage films on a PET substrate with 20 μm diameter microhole. The diode effect is quantified in terms of the rectification ratio. Effects of cationic and anionic guest species on the rectification effect are investigated. Cationic guest such as Cu^{2+}, Co^{2+}, and Ag^{+} only gradually enter the micropore space presumably due to cation exclusion. All three types of cation show a similar rectification minimum at approximately 0.5 mM, which is linked to the ingress and surface attachment of the cationic species. In contrast, anionic guest species such as indigo carmine produce a rectification minimum already at 0.5 μM and this is attributed to the blocking effect of bound indigo carmine in micropores. With increasing concentration of indigo carmine

microchannels become more active again possibly due to increased mobility with most binding sites occupied.

This exploratory study raises more questions about the ability of the virus surface to interact with specific cations and anions. More work will be required to further explore effects of electrolytes and surface modifications. The observed rectification effects are currently too weak to really develop into realistic applications (e.g. for desalination or for sensors), but improvements in the semi-permeability of the phage materials are possible and specificity in binding could be high. In the future, specifically modified phage materials could be employed in membrane separation (e.g. water purification) but also developed with sensor function for neutral, anionic, or cationic species.

Acknowledgement

B.R.P. would like to thank the Indonesian Endowment (LPDP RI) for a PhD scholarship. This work benefited from the use of the SasView application, originally developed under NSF award DMR-0520547. SasView contains code developed with funding from the European Union's Horizon 2020 research and innovation programme under the SINE2020 project, grant agreement No 654000. KSK and PK thank the Polish National Science Centre under the SONATA 13 grant UMO 2017/26/D/ST5/00980. J.A.B. thanks the Engineering and Physical Sciences Research Council for support (EP/L016354/1).

References

(1) Krajina, B.A.; Proctor, A.C.; Schoen, A.P.; Spakowitz, A.J.; Heilshorn, S.C. Biotemplated synthesis of inorganic materials: An emerging paradigm for nanomaterial synthesis inspired by nature. *Prog. Mater. Sci*. **2018**, *91*, 1–23.

(2) Zhao, X.; Lin, Y.; Wang, Q. Phage robust Virus-based scaffolds for tissue engineering applications. *Wiley Interdisciplinary Rev. Nanomedicine Nanobiotechnology* **2015**, *7*, 534–547.

(3) Smith, G.P.; Petrenko, V.A. Phage display. *Chem. Rev.* **1997**, *97*, 391–410.

(4) Johnsson, K.; Ge, L. Phage display of combinatorial peptide and protein libraries and their applications in biology and chemistry. Combinatorial chemistry in biology. *Current Topics in Microbioogy and Immunology*, **1999**, *243*, 87–105.

(5) Goldman, E.R.; Pazirandeh, M.P.; Mauro, J.M.; King, K.D.; Frey, J.C.; Anderson, G.P. Phage-displayed peptides as biosensor reagents. *J. Molecular Recognition* **2000**, *13*, 382–387.

(6) Arter, J.A.; Taggart, D.K.; McIntire, T.M.; Penner, R.M.; Weiss, G.A. Virus-PEDOT Nanowires for Biosensing. *Nano Lett.* **2010**, *10*, 4858–4862.

(7) Lee, H.Y.; Choi, J.S.; Guruprasath, P.; Lee, B.H.; Cho, Y.W. An Electrochemical Biosensor Based on a Myoglobin-specific Binding Peptide for Early Diagnosis of Acute Myocardial Infarction. *Anal. Sci.* **2015**, *31*, 699–704.

(8) Wang, D.H.; Hinkley, T.; Chen, J.H.; Talbert, J.N.; Nugen, S.R. Phage based electrochemical detection of Escherichia coli in drinking water using affinity reporter probes. *Analyst* **2019**, *144*, 1345–1352.

(9) Szot-Karpinska, K.; Lesniewski, A.; Jonsson-Niedziolka, M.; Marken, F.; Niedziolka-Jonsson, J. Electrodes modified with bacteriophages and carbon nanofibres for cysteine detection. *Sens. Actuators B Chem.* **2019**, *287*, 78–85.

(10) Putra, B.R.; Aoki, K.J.; Chen, J.Y.; Marken, F. Cationic Rectifier Based on a Graphene Oxide-Covered Microhole: Theory and Experiment. *Langmuir* **2019**, *35*, 2055–2065.

(11) Madrid, E.; Cottis, P.; Rong, Y.Y.; Rogers, A.T.; Stone, J.M.; Malpass-Evans, R.; Carta, M.; McKeown, N.B.; Marken, F. Water desalination concept using an ionic rectifier based on a polymer of intrinsic microporosity (PIM). *J. Mater. Chem. A* **2015**, *3*, 15849–15853.

(12) Mohan, K.; Weiss, G.A. Chemically Modifying Viruses for Diverse Applications. *ACS Chem. Biol.* **2016**, *11*, 1167–1179.

(13) Tjhung, K.F.; Burnham, S.; Anany, H.; Griffiths, M.W.; Derda, R. Rapid Enumeration of Phage in Monodisperse Emulsions. *Anal. Chem.* **2014**, *86*, 5642–5648.

(14) Garg, P. Filamentous bacteriophage: A prospective platform for targeting drugs in phage-mediated cancer therapy. *J. Cancer Res. Therapeutics* **2019**, *15*, S1–S10.

(15) Muzard, J.; Platt, M.; Lee, G.U. M13 Bacteriophage-Activated Superparamagnetic Beads for Affinity Separation. *Small* **2012**, *8*, 2403–2411.

(16) Marvin, D.A.; Hale, R.D.; Nave, C.; Helmer Citterich, M. Molecular models and structural comparisons of native and mutant class I filamentous bacteriophages: Ff (fd, f1, M13), If1 and Ike. *J. Molecular Biology* **1994**, *235*, 260–286.

(17) Chung, W.J.; Lee, D.Y.; Yoo, S.Y. Chemical modulation of M13 bacteriophage and its functional opportunities for nanomedicine. *Internat. J. Nanomedicine* **2014**, *9*, 5825–5836.

(18) Lee, B.Y.; Zhang, J.X.; Zueger, C.; Chung, W.J.; Yoo, S.Y.; Wang, E.; Meyer, J.; Ramesh, R.; Lee, S.W. Virus-based piezoelectric energy generation. *Nature Nanotechnol.* **2012**, *7*, 351–356.

(19) Jazwinski, S.M.; Marco, R.; Kornberg, A. A coat protein of the bacteriophage M13 virion participates in membrane-oriented synthesis of DNA. *PNAS* **1973**, *70*, 205–209.

(20) Cao, B.R.; Xu, H.; Mao, C.B. Transmission Electron Microscopy as a Tool to Image Bio-Inorganic Nanohybrids: The Case of Phage-Gold Nanocomposites. *Microsc Res Tech.* **2011**, *74*, 627–635.

(21) Atkins, P.W.; de Paula, J., *Physical Chemistry*, Oxford University Press, Oxford, 2006, p. 168.

(22) Madrid, E.; Rong, Y.Y.; Carta, M.; McKeown, N.B.; Malpass-Evans, R.; Attard, G.A.; Clarke, T.J.; Taylor, S.H.; Long, Y.T.; Marken, F. Metastable Ionic Diodes Derived from an Amine-Based Polymer of Intrinsic Microporosity. *Angew. Chem. Inter. Ed.* **2014**, *53*, 10751–10754.

(23) www.sasview.org.

(24) Specthrie, L.; Bullitt, E.; Horiuchi, K.; Model, P.; Russel, M.; Makowski, L. Construction of a microphage variant of filamentous bacteriophage. *J. Molecular Biology* **1992**, *228*, 720–724.

(25) Brown, R.; Madrid, E.; Castaing, R.; Stone, J.M.; Squires, A.M.; Edler, K.J.; Takashina, K.; Marken, F. Free-Standing Phytantriol Q(224) Cubic-Phase Films: Resistivity Monitoring and Switching. *ChemElectroChem* **2017**, *4*, 1172–1180.

(26) Aaronson, B.D.B.; Wigmore, D.; Johns, M.A.; Scott, J.L.; Polikarpov, I.; Marken, F. Anionic diode Cellulose ionics: switching ionic diode responses by surface charge in reconstituted cellulose films. *Analyst* **2017**, *142*, 3707–3714.

(27) Mathwig, K.; Aaronson, B.D.B.; Marken, F. Ionic transport in microhole fluidic diodes based on asymmetric ionomer film deposits. *ChemElectroChem* **2018**, *5*, 897–901.

(28) Tshwenya, L.; Marken, F.; Arotiba, O.A. Carbon nanofibers provide a cationic rectifier material: specific electrolyte effects, bipolar reactivity, and prospect for desalination. *ChemElectroChem* **2019**, *6*, 3145–3153.

(29) He, D.P.; Madrid, E.; Aaronson, B.D.B.; Fan, L.; Doughty, J.; Mathwig, K.; Bond, A.M.; McKeown, N.B.; Marken, F. A Cationic Diode Based on Asymmetric Nafion Film Deposits. *ACS Appl. Mater. Interfaces* **2017**, *9*, 11272–11278.

(30) Huang, S.N.; Qi, J.F.; deQuilettes, D.W.; Huang, M.T.; Lin, C.W.; Bardhan, N.M.; Dang, X.N.; Bulovic, V.; Belcher, A.M. M13 Virus-Based Framework for High Fluorescence Enhancement. *Small* **2019**, *15*, 1901233.

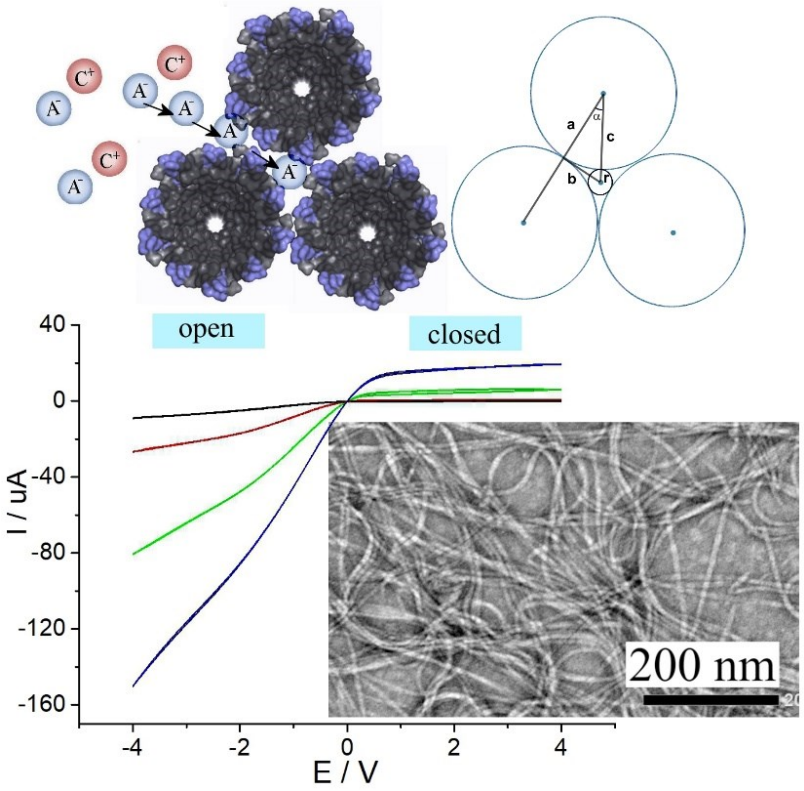

Graphical Abstract